



# Synthesis and characterization of SrBAIO<sub>4</sub>:Eu<sup>3+</sup> phosphor toward the healthy lighting for w-LEDs application

Zhen Li<sup>1</sup> and Ziquan Guo<sup>1,\*</sup>

<sup>1</sup> Fujian Engineering Research Center for Solid-State Lighting, Department of Electronic Science, Xiamen University, Xiamen 361005, China

Received: 22 September 2022

Accepted: 3 January 2023

Published online:

4 February 2023

© The Author(s), under exclusive licence to Springer Science+Business Media, LLC, part of Springer Nature 2023

## ABSTRACT

A series of orange–red-emitting Eu<sup>3+</sup>-doped Sr<sub>1-x</sub>BAIO<sub>4</sub> (0 ≤ x ≤ 0.13) phosphors via the solid-state synthesis and the luminescent and thermal properties are comprehensively investigated. Through the experiment, it is discovered that the optimal concentration of Eu<sup>3+</sup> in Sr<sub>1-x</sub>BAIO<sub>4</sub>:xEu<sup>3+</sup> phosphors belong to x = 0.09 and can be excited by near-ultraviolet wavelength of 394 nm (<sup>7</sup>F<sub>0</sub>–<sup>5</sup>L<sub>6</sub>). The Sr<sub>0.91</sub>BAIO<sub>4</sub>:0.09Eu<sup>3+</sup> phosphors possess a good thermal stability, of which the emission intensity at 150 °C can maintain 75.89% of the initial value (25 °C). The circadian action and color rendering of near-ultraviolet white light-emitting diodes (LEDs) are studied, and the optimum circadian action factor (CAF) decreases 11.9% compared to that of the standard light source under a correlated color temperature (CCT) of 7018 K. Finally, it is recommended that the SrBAIO<sub>4</sub>:Eu<sup>3+</sup> phosphors applied in near-ultraviolet white light-emitting diodes show great potentials for their applications in the healthy lighting.

## 1 Introduction

In recent years, the environmental problems, such as the global warming, the climate change, the depletion of nature resources, and the pollution have become a global challenge. The current conditions encourage the urgent need for the alternate as well as clean energy production. The rare-earth ion-based inorganic luminescent materials with excellent luminescent properties have been widely studied and used in various application fields, such as lighting, back-lighting for displays, and visible light communication

(VLC) among others [1–3]. White light-emitting diodes (w-LEDs), as a new generation of light source, possess several typical merits, for instance, environment-friendliness, low electricity consumption, long life span, small volume, and fast response [4–6]. The commercial w-LEDs are mainly composed of blue InGaN-based LEDs and broadband yellow-emitting Y<sub>3</sub>Al<sub>5</sub>O<sub>12</sub>:Ce<sup>3+</sup> (YAG:Ce<sup>3+</sup>) phosphors [7]. However, the deficiency in the red component of w-LEDs leads to a poor color-rendering index (CRI) and high correlated color temperature (CCT) [8, 9]. In addition, their spectra are far beyond the sunlight and thus, the

Address correspondence to E-mail: zqguo@xmu.edu.cn

w-LEDs devices are unsuitable for the indoor lighting. In order to overcome these issues, many researchers focused on w-LEDs with lower CCT and higher CRI [10, 11] and provided several solutions. Among them, a near-ultraviolet (NUV) LED coated with tricolor phosphors to fabricate w-LEDs is regarded as a potential candidate.

The borate crystals are excellent host structures for phosphors due to their inherent properties of large bandgap and covalent bond energy. Recently, different tricolor borate phosphors excited by NUV-LEDs have been reported, such as blue phosphors like  $\text{NaSrBO}_3:\text{Ce}^{3+}$  [12], green phosphors such as  $\text{Sr}_2\text{MgB}_2\text{O}_6:\text{Tb}^{3+}$ ,  $\text{Li}^+$  [13], and red phosphors like  $\text{SrAl}_2\text{B}_2\text{O}_7:\text{Eu}^{3+}$  [14]. The aluminum borate phosphors have been widely investigated recently owing to their lower synthetic temperature, excellent physical, and chemical stabilities [15, 16]. The synthesis temperature of  $\text{Eu}^{3+}$ -doped boron-contained phosphor is generally less than 1000 °C and crystal particle size is generally around 10  $\mu\text{m}$ . In the meanwhile, the  $\text{Eu}^{3+}$ -doped boron-contained phosphors have the good quantum yield and generally exceed 10%, for instance, the  $\text{CaB}_6\text{O}_{10}:\text{Eu}^{3+}$  phosphor is 27% [17] and the  $\text{Ba}_3\text{Lu}_2\text{B}_6\text{O}_{15}:\text{Eu}^{3+}$  phosphor is 17% [18]. The emission peaks have the band around 593 nm belong to  ${}^5\text{D}_0\text{-}{}^7\text{F}_1$  transition and the band around 612 nm belong to  ${}^5\text{D}_0\text{-}{}^7\text{F}_2$  transition. According to the Judd–Ofelt theory [19, 20], the prohibited electric dipole transition  ${}^5\text{D}_0\text{-}{}^7\text{F}_2$  is very sensitive to the lattice environment, but the magnetic dipole transition  ${}^5\text{D}_0\text{-}{}^7\text{F}_1$  is not affected by the lattice environment of  $\text{Eu}^{3+}$  ions. If  $\text{Eu}^{3+}$  occupies inversion center sites in the situation, the magnetic dipole transition  ${}^5\text{D}_0\text{-}{}^7\text{F}_1$  is the main transition, showing orange–red emission. Conversely, the electric dipole transition  ${}^5\text{D}_0\text{-}{}^7\text{F}_2$  is the main transition mode. By mixing with phosphors of other colors, it is possible to fabricate white LEDs with excellent performance in NUV excitation or blue excitation. To the best of our knowledge, there are no reports in literatures devoted to luminescence properties of  $\text{Eu}^{3+}$ -doped  $\text{SrBAIO}_4$  phosphors.

In this paper, we report on novel orange–red  $\text{SrBAIO}_4$ -based borate phosphors, which are obtained at 820 °C by conventional solid-state reaction methods. The concentration quenching, critical transfer distance, as well as Commission Internationale de

l’Eclairage (CIE) chromaticity coordinates of  $\text{Eu}^{3+}$ -doped  $\text{SrBAIO}_4$  phosphors are also analyzed. We have also carried out spectral optimization on circadian action factor (CAF) and color rendering of white light based on proposed  $\text{Eu}^{3+}$ -doped  $\text{SrBAIO}_4$  phosphors. All results indicate that the  $\text{Eu}^{3+}$ -doped  $\text{SrBAIO}_4$  phosphor is a kind of potential orange–red-emitting materials possibly applied in the healthy lighting fields.

## 2 Experimental

In this experiment, a series of  $\text{Sr}_{1-x}\text{BAIO}_4:x\text{Eu}^{3+}$  phosphors ( $x = 0.03, 0.05, 0.07, 0.09, 0.11, \text{ and } 0.13$ , respectively) were fabricated via a conventional high-temperature solid-state reaction method. The reagents of  $\text{SrCO}_3$  (AR),  $\text{H}_3\text{BO}_3$  (AR),  $\text{Al}_2\text{O}_3$  (AR), and  $\text{Eu}_2\text{O}_3$  (4 N) were mixed in the stoichiometric proportion and put together in an agate mortar. The amount of  $\text{H}_3\text{BO}_3$  was added in excess of 3% to compensate its evaporation losses during the synthesis process. Then, the mixtures were transferred to a corundum crucible, heated in a muffle furnace at 350 °C for 3 h and subsequently annealed at 820 °C for 12 h in the air.

The X-ray diffraction (XRD) patterns were applied for the crystal analysis using the Panalytical X-pert PRO Diffractometer with  $\text{Cu K}\alpha$  (40.0 kV, 30.0 mA) radiation ( $\lambda = 1.5418 \text{ \AA}$ ). The thermogravimetric analysis (DTA) and the derivative thermogravimetric (DTG) curves dependent on temperature were obtained by an STA 449 F5 simultaneous thermo-analytical instrument. The photoluminescence excitation (PLE) and photoluminescence (PL) spectra were tested by a Hitachi F-7000 spectrometer equipped with a 150-W Xenon lamp as an excitation source. The PL decays and the temperature-dependent PL spectra were recorded by an OmniFlow 990 spectrometer. A Keysight Technologies B2912A instrument was used to supply the electrical current for the LED chips. The surface morphology and grain size of as-prepared samples were observed by a Hitachi SU-70 field-emission scanning electron microscope (FE-SEM). The spectral calculation for circadian action and color-rendering properties was done using the self-designed calculation software. All measurements were performed at room temperature.

### 3 Results and discussion

#### 3.1 Phase formation of $\text{Sr}_{1-x}\text{BaAlO}_4:x\text{Eu}^{3+}$ phosphors

Figure 1 provides DTA/DTG curves of the stoichiometric mixture of  $\text{SrCO}_3$ ,  $\text{H}_3\text{BO}_3$ , and  $\text{Al}_2\text{O}_3$ , which are heated from the room temperature to 900 °C with a heating rate of 10 °C/min in the air. The weight loss before 550 °C is mainly contributed to the release of  $\text{CO}_2$  and  $\text{H}_2\text{O}$  from the decomposition of starting materials. The DTG shows an obvious peak at about 820 °C, corresponding to a quick weight loss in the moment temperature, and it determines the sintering temperature of  $\text{SrBaAlO}_4:\text{Eu}^{3+}$  to be 820 °C. The SEM image shown in the inset of Fig. 1 reveals the surface morphology of phosphors, and the well-separated particles are approximately 4–8  $\mu\text{m}$ .

Figure 2a illustrates the schematic of the  $\text{SrBaAlO}_4$  crystal structure is orthorhombic with a space group of  $Pccn$ , featuring the lattice parameters of  $a = 15.17 \text{ \AA}$ ,  $b = 8.86 \text{ \AA}$ ,  $c = 5.48 \text{ \AA}$ , and  $V = 736.55 \text{ \AA}^3$  [21]. It is obvious that  $\text{Sr}^{2+}$  and  $\text{Al}^{3+}$  ions in  $\text{SrBaAlO}_4$  are sixfold (CN = 6,  $r = 1.18 \text{ \AA}$ ) and fourfold (CN = 4,  $r = 0.39 \text{ \AA}$ ) coordinated by  $\text{O}^{2-}$  ions. However,  $\text{Eu}^{3+}$  has four ways of coordination and ionic radius (CN = 6,  $r = 0.947 \text{ \AA}$ , CN = 7,  $r = 1.01 \text{ \AA}$ , CN = 8,  $r = 1.066 \text{ \AA}$ , and CN = 9,  $r = 1.12 \text{ \AA}$ ). Due to the coordination number and similar ionic radius, we deduce that  $\text{Eu}^{3+}$  ions (CN = 6,  $r = 0.947 \text{ \AA}$ ) will substitute  $\text{Sr}^{2+}$  (CN = 6,  $r = 1.18 \text{ \AA}$ ). XRD patterns of  $\text{SrBaAlO}_4$  and  $\text{Sr}_{1-x}\text{BaAlO}_4:x\text{Eu}^{3+}$  ( $x = 0.03, 0.05, 0.07, 0.09, 0.11, \text{ and } 0.13$ ) phosphors with different  $\text{Eu}^{3+}$

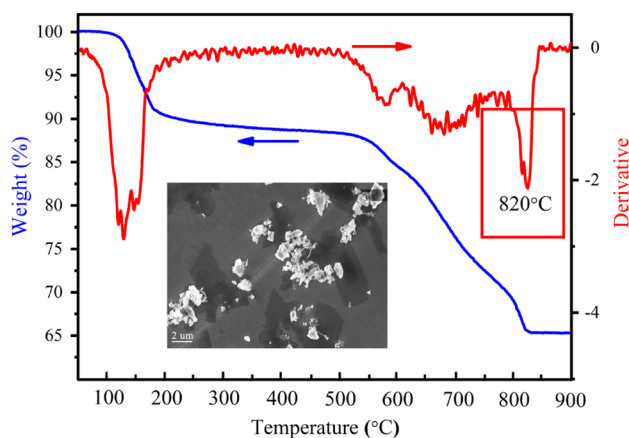


**Fig. 1** The DTA / DTG curves of as-synthesized  $\text{SrBaAlO}_4$  with the heating rate of 10 °C/min and the inset shows the SEM image of the phosphor

doping contents ( $x$ ) as shown in Fig. 2b. It can be noticed that almost all the diffraction peaks can be well indexed to the standard ICSD-28107 card with seldom interfering peaks [21], suggesting that a pure crystalline compound is obtained. It indicates that doped  $\text{Eu}^{3+}$  doping has not led to obvious changes in the host structure.

#### 3.2 Luminescence properties of $\text{Sr}_{1-x}\text{BaAlO}_4:x\text{Eu}^{3+}$ phosphors

The photoluminescence excitation (PLE) and photoluminescence (PL) spectra of  $\text{Sr}_{1-x}\text{BaAlO}_4:x\text{Eu}^{3+}$  phosphors are presented in Fig. 3. A series of excitation bands can be observed in PLE spectra monitored at 593 nm, as presented in Fig. 3a. At the same time, the electronic energy-level diagram for  $\text{Eu}^{3+}$  in  $\text{SrBaAlO}_4$  is sketched in Fig. 3d. It can be observed that a strong absorption band from 230 to 300 nm centered at 256 nm that corresponds to the charge transfer band (CTB) from oxygen ( $\text{O}^{2-}$ ) to the  $\text{Eu}^{3+}$ . The other sharp peaks centered at 319 nm ( ${}^7\text{F}_0 - {}^5\text{H}_6$ ), 362 nm ( ${}^7\text{F}_0 - {}^5\text{D}_4$ ), 382 nm ( ${}^7\text{F}_0 - {}^5\text{L}_7$ ), 394 nm ( ${}^7\text{F}_0 - {}^5\text{L}_6$ ), 417 nm ( ${}^7\text{F}_0 - {}^5\text{D}_3$ ), 465 nm ( ${}^7\text{F}_0 - {}^5\text{D}_2$ ), and 532 nm ( ${}^7\text{F}_0 - {}^5\text{D}_1$ ), respectively, in combination with Fig. 3a.

The PL spectra of  $\text{Sr}_{1-x}\text{BaAlO}_4:x\text{Eu}^{3+}$  phosphors are displayed in Fig. 3c, when they are excited by various excitations, and the results show that the best excitation wavelength of  $\text{Sr}_{0.91}\text{BaAlO}_4:0.09\text{Eu}^{3+}$  phosphors is 394 nm at the NUV bands. On the other hand, the PL spectra, excited by 394 nm, indicate that this phosphor exhibits a yellow emission at 593 nm and a red emission at 614 nm as shown in Fig. 3b. These two peaks are attributed to  ${}^5\text{D}_0 - {}^7\text{F}_1$  and  ${}^5\text{D}_0 - {}^7\text{F}_2$  transitions of  $\text{Eu}^{3+}$  ions. The other sharp peaks centered at 652 nm ( ${}^5\text{D}_0 - {}^7\text{F}_3$ ) and 703 nm ( ${}^5\text{D}_0 - {}^7\text{F}_4$ ). Since the  $\text{Eu}^{3+}$  occupies inversion center sites in the situation, according to the Judd–Ofelt theory,  ${}^5\text{D}_0 - {}^7\text{F}_1$  transition should be relatively strong to  ${}^5\text{D}_0 - {}^7\text{F}_2$  transition. Therefore,  $\text{Sr}_{1-x}\text{BaAlO}_4:x\text{Eu}^{3+}$  phosphors mainly radiate an orange–red emission under the NUV excitation.

In order to obtain the phosphors with the brightest emission  $\text{Sr}_{1-x}\text{BaAlO}_4:x\text{Eu}^{3+}$  phosphors ( $x = 0.03$  to 0.13 with an increment of 0.02) are synthesized. The PL spectra of these phosphors under the excitation of 394 nm are plotted in Fig. 4a. It can be seen that the emission intensity rises first and is peaked at  $x = 0.09$  with the increasing concentration of  $\text{Eu}^{3+}$  ions. As the

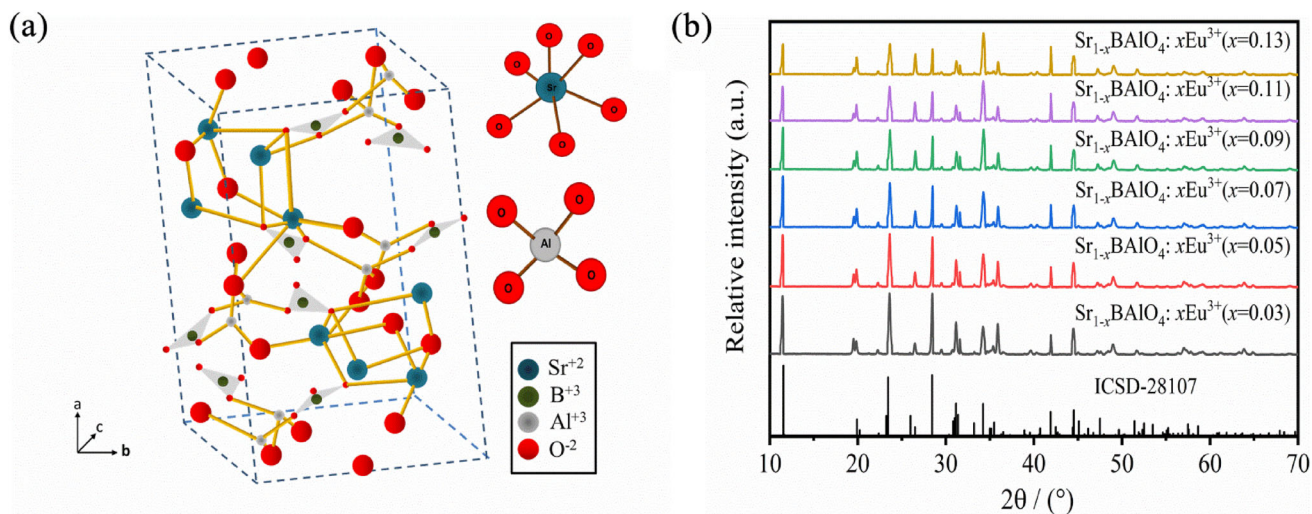


**Fig. 2** **a** The crystal structure of SrBAIO<sub>4</sub> (ICSD-28107) and **b** the XRD patterns of Sr<sub>1-x</sub>BAIO<sub>4</sub>:xEu<sup>3+</sup> (x = 0.03, 0.05, 0.07, 0.09, 0.11, and 0.13, respectively) phosphor

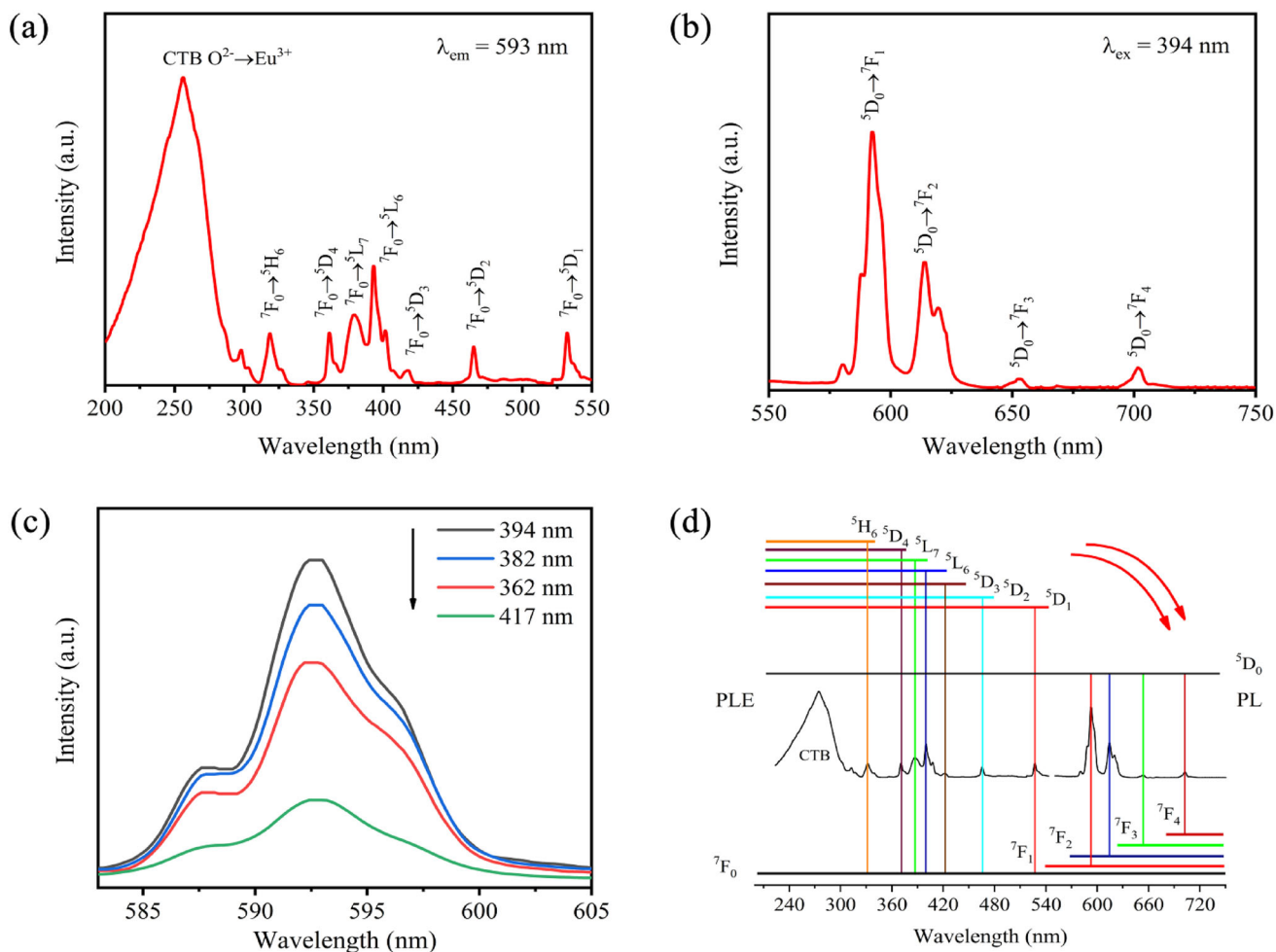


**Fig. 3** **a** Excitation ( $\lambda_{em} = 593$  nm) spectra. **b** Emission ( $\lambda_{ex} = 394$  nm) spectra. **c** Luminescence spectra at various excitation wavelengths. **d** Electronic energy-level scheme for Eu<sup>3+</sup> in SrBAIO<sub>4</sub>



concentration of  $\text{Eu}^{3+}$  continues to increase, the PL intensity gradually decreases due to concentration quenching effects. This quenching action is frequently ascribed to non-radiative energy migration of  $\text{Eu}^{3+}$  ions. Accordingly, it is determined that the optimal concentration of  $\text{Eu}^{3+}$  in series of phosphors is  $x = 0.09$ .

The mechanism of energy transfer phosphors was expounded by Blasse [22]. The concentration quenching of  $\text{Eu}^{3+}$  ions is closely related to critical transfer distance  $R_c$ , which can be calculated by the following equation:

$$R_c = 2 \left[ \frac{3V}{4\pi X_c N} \right]^{\frac{1}{3}}, \tag{1}$$

where  $N$  is the number of cations in unit cells,  $X_c$  is the optimal concentration, and  $V$  is the volume of the unit cell. For the  $\text{SrBAIO}_4$  structure, the values of  $N$ ,  $X_c$ , and  $V$  are 8, 0.09, and  $736.55 \text{ \AA}^3$  [21], respectively. Substituting these parameters into Eq. (1),  $R_c$  is determined to be  $6.25 \text{ \AA}$ . As we know, critical transfer distance  $R_c$  is generally less than  $5 \text{ \AA}$  [23], for this reason the multipolar electrical interaction is involved in the energy transfer process.

According to Dexter theory [24–26], the fluorescence mechanism of  $\text{Eu}^{3+}$  in  $\text{SrBAIO}_4:\text{Eu}^{3+}$  phosphors is the multiple–multiple interaction, and the correlation of emission intensity ( $I$ ) and doping concentration ( $x$ ) can be inferred from the following equation:

$$I/x = K [1 + \beta(x)^Q]^{-1}, \tag{2}$$

where  $x$  is the activator concentration and  $K$  and  $\beta$  are two constants under the same excitation condition for the host crystal. The value of  $Q$  can be 6, 8, and 10 for dipole–dipole (d-d), dipole–quadrupole (d-p), and quadrupole–quadrupole (q-q) interaction, respectively. By converting Eq. (2) to obtain the value of  $Q$ , a curve of  $\lg(x)$  versus  $\lg(I/x)$  is plotted in Fig. 4b, where the slope of fitting line equals to  $-1.87$ . Thus, the value of  $Q$  can be deduced from Eq. (2) as 5.6, and this value is approximately equal to 6. Therefore, it can be inferred that the d-d interaction is major concentration quenching mechanism of  $\text{Eu}^{3+}$  emission in  $\text{Sr}_{1-x}\text{BAIO}_4:x\text{Eu}^{3+}$  phosphors.

### 3.3 Thermal properties of $\text{Sr}_{1-x}\text{BAIO}_4:x\text{Eu}^{3+}$ phosphors

In general, the thermal stability of rare-earth phosphors is one of the key parameters in commercial applications. Figure 5a shows the typical relative emission intensity of  $\text{Sr}_{0.91}\text{BAIO}_4:0.09\text{Eu}^{3+}$  phosphors as a function of from 25 to 150 °C. Due to the thermal quenching of emission intensity caused by phonon interaction, as can be seen from the inset in Fig. 5a, the intensity of emission decreases to 75.89% when the temperature is up to 150 °C. The result shows that the  $\text{Sr}_{0.91}\text{BAIO}_4:0.09\text{Eu}^{3+}$  phosphor has better thermal stability performance than those of many phosphors in the literatures [27, 28].

To further analyze the temperature-dependent phenomenon, the activation energy for describing the

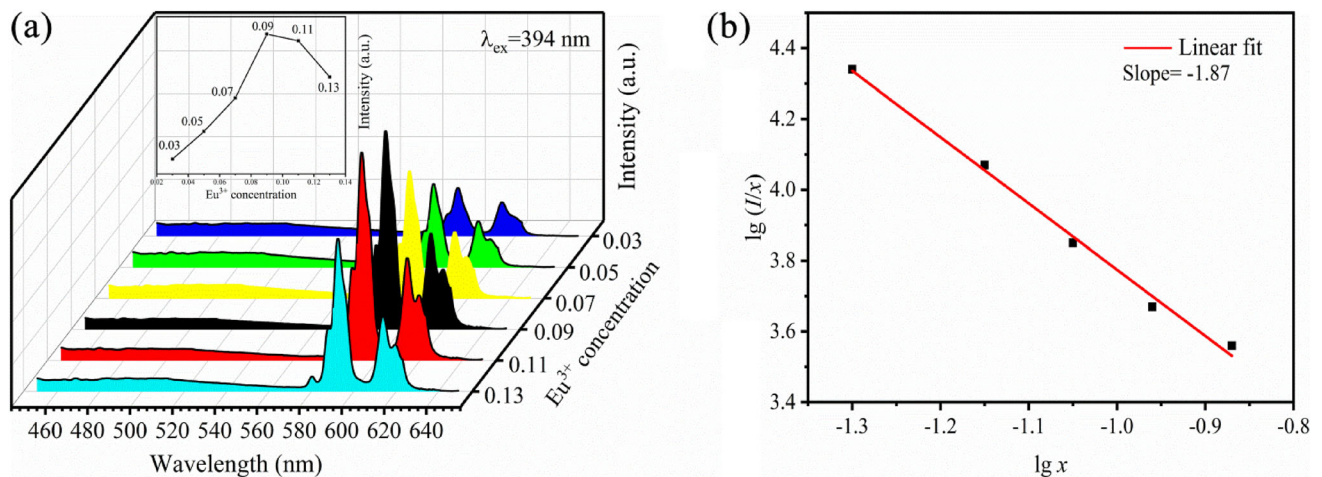


**Fig. 4** **a** The emission intensity  $\text{Sr}_{1-x}\text{BAIO}_4:x\text{Eu}^{3+}$  as a function of  $\text{Eu}^{3+}$  concentration. **b** The plot of  $\lg(x)$  versus  $\lg(I/x)$  for  $\text{Sr}_{1-x}\text{BAIO}_4:x\text{Eu}^{3+}$  phosphors ( $\lambda_{\text{ex}} = 394 \text{ nm}$ )

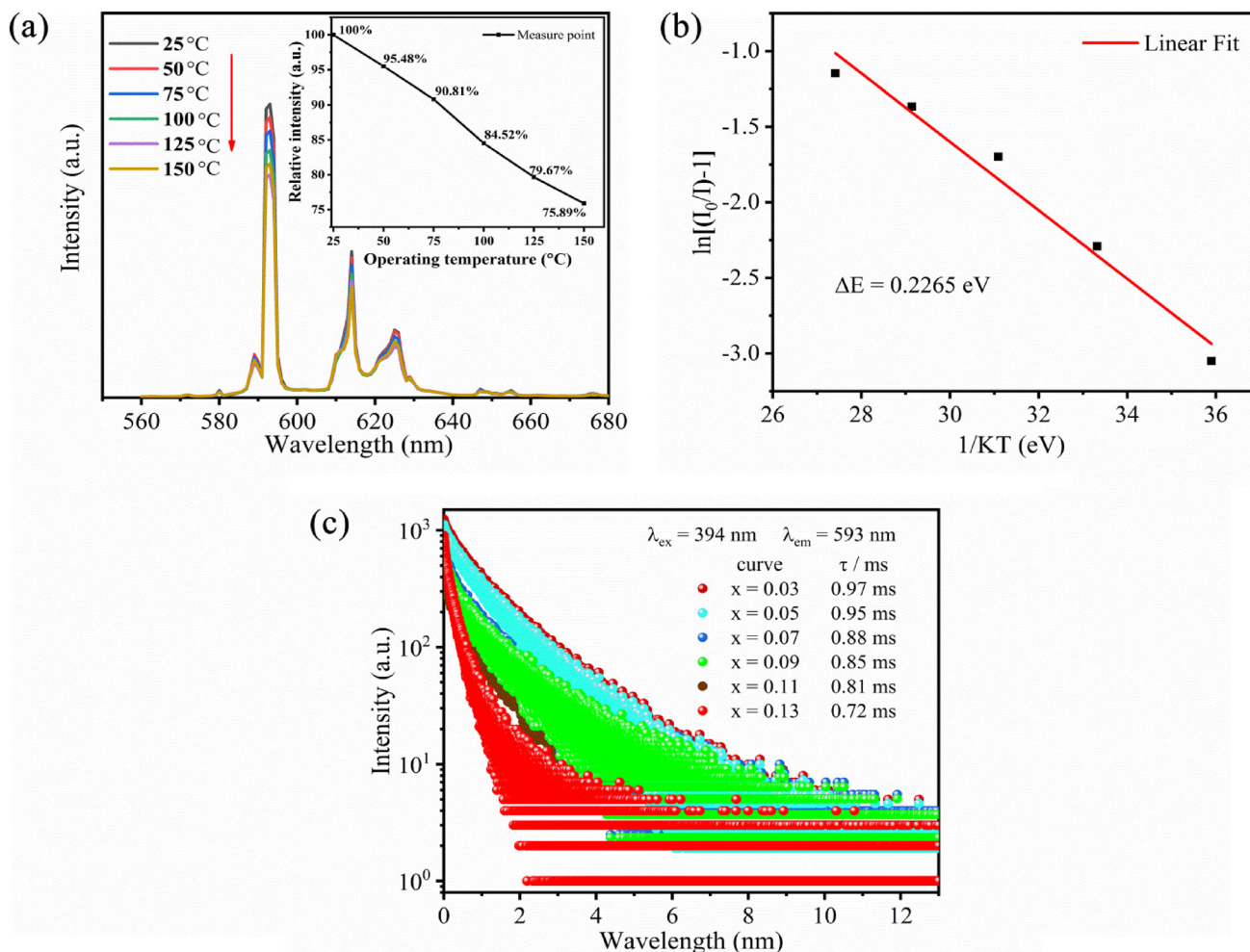


**Fig. 5** **a** Temperature-dependent PL spectra excited by 394 nm (the insert shows the attenuation ration of emission intensity). **b** Activation energy for thermal quenching of

thermal quenching is determined by the well-known Arrhenius equation [29]:

$$I(T) = \frac{I_0}{1 + c \cdot \exp\left(-\frac{\Delta E}{kT}\right)}, \quad (3)$$

where  $I(T)$  is the emission intensity operating temperatures  $T$ ,  $I_0$  is the initial emission intensity at 25 °C,  $c$  is a constant,  $k$  is the Boltzmann constant with a value of  $8.62 \times 10^{-5} \text{ eV} \cdot \text{K}^{-1}$ , and  $\Delta E$  is the activation energy. Figure 5b shows the linear fitting relationship of  $\ln[(I_0 / I_T)-1]$  versus  $1 / (kT)$ . Consequently, the activation energy of thermal quenching can be calculated to be 0.2265 eV. It is higher than the reported data for  $\text{Ba}_6\text{Gd}_2\text{Ti}_4\text{O}_{17}:\text{Eu}^{3+}$  (0.144 eV),  $\text{NaYGeO}_4:\text{Eu}^{3+}$  (0.213 eV), and  $\text{BaLaLiTeO}_6:\text{Eu}^{3+}$  (0.220 eV) [30–32]. The obtained parameters indicate

$\text{Sr}_{0.91}\text{Ba}_{104}:\text{0.09Eu}^{3+}$  phosphors under 394 nm excitation and monitored at 593 nm. **c** Decay curves of  $\text{Sr}_{1-x}\text{Ba}_{104}:\text{xEu}^{3+}$  ( $x = 0.03, 0.05, 0.07, 0.09, 0.11,$  and  $0.13$ ) phosphors

that  $\text{Sr}_{1-x}\text{Ba}_{104}:\text{xEu}^{3+}$  phosphors have good thermal stability for potential application in NUV-LEDs.

To further confirm the lifetime of the optimum concentration of  $\text{Eu}^{3+}$  in  $\text{Sr}_{0.91}\text{Ba}_{104}:\text{0.09Eu}^{3+}$  phosphor, the PL decay curve of the phosphor under 394 nm is recorded at the room temperature.

The decay curves can be well fitted by a double exponential function:

$$I_t = I_0 + A_1 \cdot \exp(-t/\tau_1) + A_2 \cdot \exp(-t/\tau_2), \quad (4)$$

where  $t$  is the time,  $I_t$  represents the luminescence intensity at time  $t$ ,  $I_0$  is the luminescence offset intensity,  $A_1$  and  $A_2$  are constants, and  $\tau_1$  and  $\tau_2$  signify the lifetime of the exponential components, respectively. The average lifetime can be calculated by the equation:

$$\tau_{av} = (A_1\tau_1 + A_2\tau_2)/(A_1\tau_1^2 + A_2\tau_2^2). \tag{5}$$

The value of  $\tau_{av}$  fitted from the  $Sr_{1-x}BaAlO_4:xEu^{3+}$  ( $x = 0.03, 0.05, 0.07, 0.09, 0.11,$  and  $0.13$ ) phosphors are calculated to be 0.97, 0.95, 0.88, 0.85, 0.81, and 0.72 ms as shown in Fig. 5c. It can be seen that the changing trend of fluorescence lifetime is opposite to the changing of doping ion concentrations.  $Sr_{0.91}BaAlO_4:0.09Eu^{3+}$  phosphor is shorter than the previously reported values in  $Eu^{3+}$  doping phosphors [33, 34]. The short lifetime indicates that the  $SrBaAlO_4:Eu^{3+}$  phosphors are appropriate for the potential application in white LEDs.

### 3.4 Quantum yield of $SrBaAlO_4:Eu^{3+}$ phosphors

The quantum yield of phosphor is a significant factor in the application for LEDs. We measured the quantum yield of the phosphor by the integrating sphere. As shown in Table 1, the quantum yield of  $Sr_{0.91}BaAlO_4:0.09Eu^{3+}$  phosphor is 13.6%, which is higher than the reference [35], but it is lower than the reference [36]. Since the present phosphor is excited by related low energy of NUV at 394 nm, whose energy is UV light at 270 nm. The UV light (190 – 280 nm) is expensive and harmful to human health, and the  $Sr_{0.91}BaAlO_4:0.09Eu^{3+}$  phosphor shows the good quantum yields at NUV light. Therefore, the  $SrBaAlO_4:Eu^{3+}$  phosphors have a potential application for w-LEDs.

### 3.5 Color properties of $Sr_{1-x}BaAlO_4:xEu^{3+}$ phosphors

The CIE chromaticity coordinates of  $Sr_{0.91}BaAlO_4:0.09Eu^{3+}$  phosphors were determined [37]. As shown in Fig. 6a, the CIE color coordinates are determined to be (0.526, 0.35), in terms of their PL spectra excited at 394 nm. In addition, color coordinates of  $Sr_{0.91}BaAlO_4:0.09Eu^{3+}$  phosphors are suited in the orange–red region of CIE chromaticity diagram. An NUV (390–400 nm) LED chip is coated with the

orange–red-emitting  $SrBaAlO_4:Eu^{3+}$ , green-emitting  $(Sr, Ba)_2SiO_4:Eu^{2+}$ , and blue-emitting  $BaMgAl_{10}O_{17}:Eu^{2+}$  phosphors by the epoxy resin adhesive. The molar ratio of the orange–red, green, and blue phosphors is 9:2:4. When the epoxy resin adhesive is cured, connected to the current source, the white LED could be lightened as shown in the insert of Fig. 6b. The results show that with the increase in the current drive forward, the spectra of w-LED get stronger and the rate of increase becomes lower, the reason is that the junction temperature of the chip increases with the enhancement of the current, which affects the luminous efficiency of the phosphor.

### 3.6 Circadian engineering and color rendering of NUV-pumped w-LEDs based on $SrBaAlO_4:Eu^{3+}$ phosphors

Recently, people gradually pay close attention to the healthy lighting related to the third type of photoreceptor called as intrinsically photosensitive retinal ganglion cells (ipRGCs), which play a key role in the formation and release of melatonin, cortisol, and other hormones. The ipRGCs are sensitive to the blue-rich light, that is to say, the blue-rich light may disturb the 24-h biological clock of human beings, namely circadian rhythms. Under this situation, the NUV-pumped w-LEDs become a good choice for the healthy lighting application owing to its not too strong but broadband blue emission for good color rendering. Generally, the circadian effects of light source can be quantified through the calculation of circadian action factor (CAF). The CAF is defined by the following equation [38]:

$$CAF = \frac{\int_{\lambda_1}^{\lambda_2} C(\lambda)S(\lambda)d\lambda}{\int_{\lambda_1}^{\lambda_2} V(\lambda)S(\lambda)d\lambda}, \tag{6}$$

where  $C(\lambda)$  is the circadian efficiency function,  $V(\lambda)$  is the photonic efficiency function, and  $S(\lambda)$  is the spectrum of w-LEDs. In this work, we study the circadian engineering and color rendering of NUV-pumped w-LEDs based on orange–red-emitting  $SrBaAlO_4:Eu^{3+}$  phosphors, green-emitting (Sr,

**Table 1** Quantum efficiencies of  $Sr_{0.91}BaAlO_4:0.09Eu^{3+}$  phosphor and references

Host, $xEu^{3+}$	Excitation wavelength (nm)	Quantum efficiency (%)	References
$Sr_{0.91}BaAlO_4:0.09Eu^{3+}$	394	13.6	Present work
$SrLa_{1.5}Mg_2W_2O_{12}:0.5Eu^{3+}$	395	8.8	[35]
$YBO_3:0.05Eu^{3+}$	270	79.7	[36]



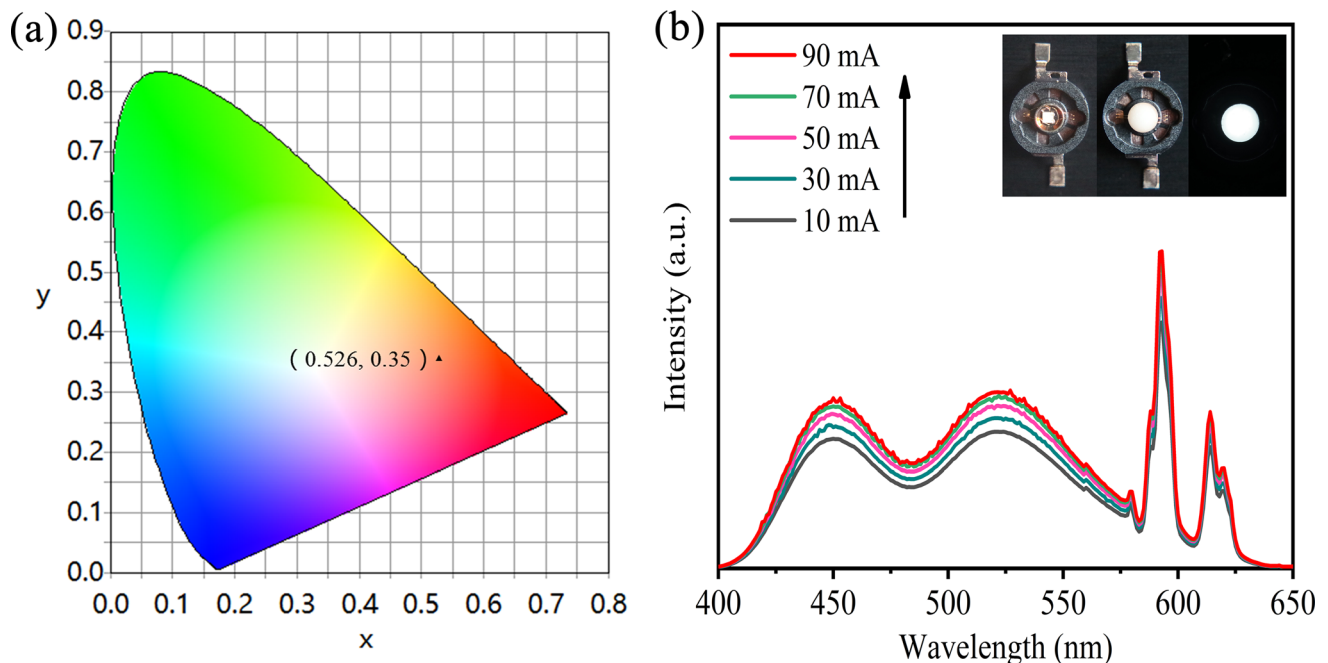


**Fig. 6** **a** Chromaticity coordinates of the  $\text{Sr}_{0.91}\text{BaAlO}_4:0.09\text{Eu}^{3+}$  phosphor in the CIE 1931 chromaticity diagram. **b** The spectra of the w-LED with different currents. The insert shows a W-LED

$\text{Ba}_2\text{SiO}_4:\text{Eu}^{2+}$ , and blue-emitting  $\text{BaMgAl}_{10}\text{O}_{17}:\text{Eu}^{2+}$  phosphors pumped by 394-nm NUV emission. The CRI and color-quality scale (CQS) [39] are used to describe the color rendering of NUV-pumped w-LEDs. By matching the spectra of the three phosphors in different proportions, the significant parameters of w-LEDs can be calculated, such as Combo-1 (CCT = 4668 K), Combo-2 (CCT = 5616 K), Combo-3 (CCT = 6244 K), and Combo-4 (CCT = 7018 K). Table 2 lists the optimum CAF, CRI, CQS, CCT, and other important parameters.

As can be found, the optimum CAF decreases -11.9% compared to the standard light source ( $\text{CAF}_r$ ) at CCT = 7018 K (Combo-4), showing great potentials in the achievement of low CAF for healthy lighting by these NUV-pumped w-LEDs based on orange-red-emitting  $\text{SrBaAlO}_4:\text{Eu}^{3+}$  phosphors. Figure 7 shows the spectra of Combo-1, Combo-2,

made by coating orange-red-emitting  $\text{SrBaAlO}_4:\text{Eu}^{3+}$  phosphors, green-emitting  $(\text{Sr}, \text{Ba})_2\text{SiO}_4:\text{Eu}^{2+}$ , and blue-emitting  $\text{BaMgAl}_{10}\text{O}_{17}:\text{Eu}^{2+}$  phosphors on a NUV (390–400 nm) chip

Combo-3, and Combo-4 with their circadian and photonic performances.

## 4 Conclusion

In this contribution, a series of orange-red emitting  $\text{Eu}^{3+}$ -doped  $\text{Sr}_{1-x}\text{BaAlO}_4$  ( $0 \leq x \leq 0.13$ ) phosphors are prepared and the luminescent, thermal, and color properties of the compounds were comprehensively investigated. The optimal concentration of  $\text{Eu}^{3+}$  in  $\text{Sr}_{1-x}\text{BaAlO}_4:x\text{Eu}^{3+}$  phosphors is  $x = 0.09$ , and the emission intensity at 150 °C can maintain 75.89% of the initial value (25 °C). For white LEDs based on orange-red-emitting  $\text{SrBaAlO}_4:\text{Eu}^{3+}$  phosphors, green-emitting  $(\text{Sr}, \text{Ba})_2\text{SiO}_4:\text{Eu}^{2+}$  and blue-emitting  $\text{BaMgAl}_{10}\text{O}_{17}:\text{Eu}^{2+}$  phosphors, the optimum CAF decreases -11.9% compared to the standard light source at CCT of 7018 K. Therefore, it is strongly

**Table 2** Some parameters of w-LEDs

Parameters	CCT (K)	LER (lm/W)	CAF	CRI	CQS	CIE(x)	CIE(y)	$\text{CAF}_r$	$\Delta$
Combo-1	4668	344	0.707	81	76	0.3544	0.3543	0.718	- 1.5%
Combo-2	5616	337	0.783	83	76	0.3297	0.3509	0.834	- 6.1%
Combo-3	6244	333	0.827	83	68	0.3155	0.3489	0.912	- 9.3%
Combo-4	7018	329	0.876	81	56	0.2998	0.3467	0.994	- 11.9%



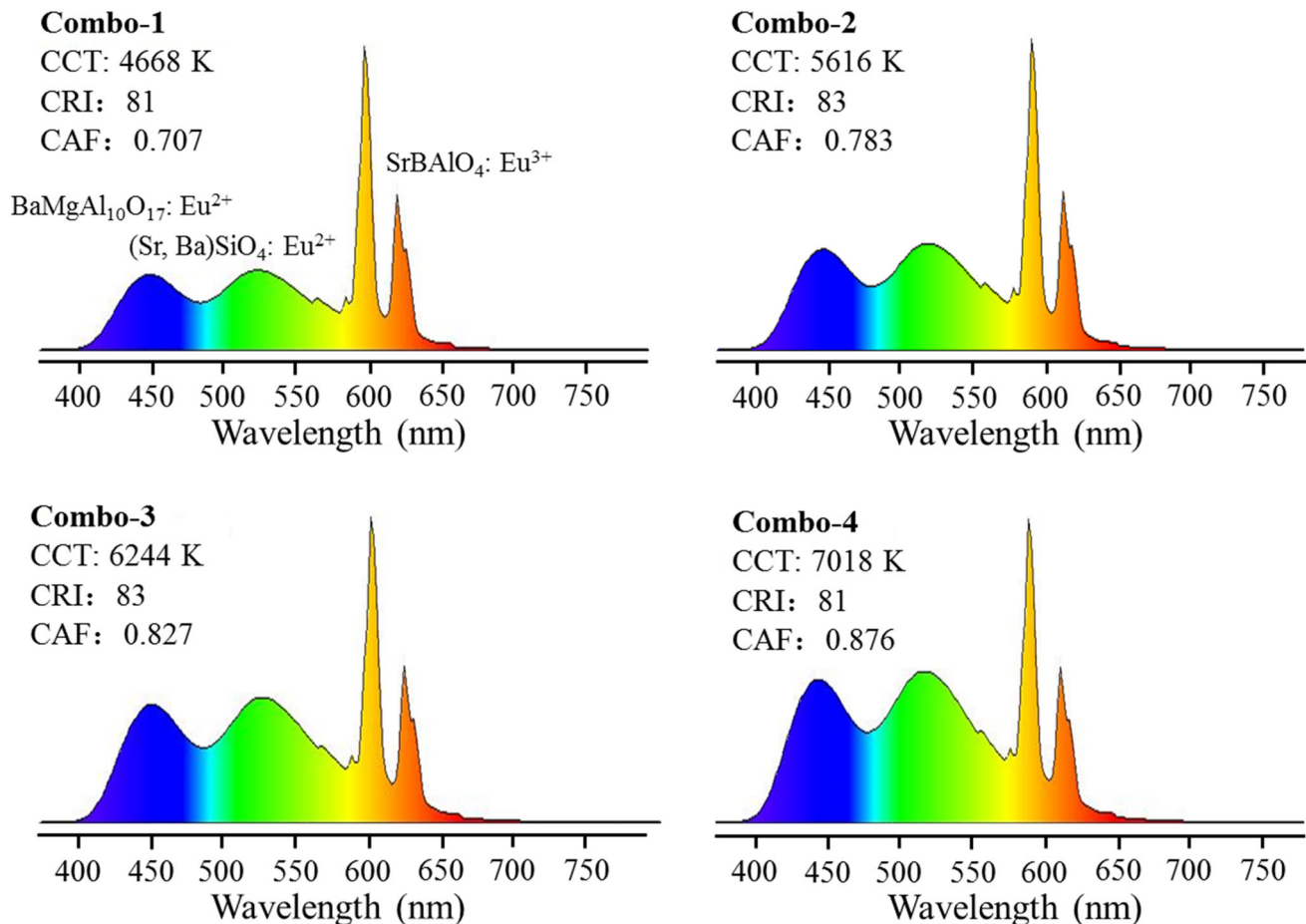


**Fig. 7** The spectra of Combo-1, Combo-2, Combo-3, and Combo-4

recommended that  $\text{SrBaAlO}_4:\text{Eu}^{3+}$  phosphors applied in near-ultraviolet white light-emitting diodes show great potential for their applications in the healthy lighting.

### Author contribution

ZG conceived and designed the experiments. ZL carried out the experiments. ZG and ZL analyzed the data and discussed the results. ZL wrote the paper.

### Funding

This work was supported by [the National Natural Science Foundation of China] (Grant No. 52202117), [the State Key Lab of Advanced Metals and Materials] (Grant No. 2022-Z09), [the Natural Science Foundation of Fujian Province] (Grant No.

2022J01065), and [the Fundamental Research Funds for the Central Universities] (Grant No. 20720220075). The authors thank the reviewers for their appreciated suggestions for this work.

### Data availability

The datasets generated during and/or analyzed during the current study are available from the corresponding author on reasonable request.

### Declarations

**Conflict of interest** All authors declare that they have no known competing financial interests or personal relationships that could have appeared to influence the work reported in this paper.

## References

- R. Vijayakumar, H. Guo, X.Y. Huang, Energy transfer and color-tunable luminescence properties of  $\text{Dy}^{3+}$  and  $\text{Eu}^{3+}$  co-doped  $\text{Na}_3\text{Sc}_2(\text{PO}_4)_3$  phosphors for near-UV LED-based warm white LEDs. *Dyes Pigments* **156**, 8–16 (2018)
- Y. Li, Q. Wei, H. Chen, Y. Wang, A novel red-emitting  $\text{Ca}_2\text{GdHf}_2\text{Al}_3\text{O}_{12}:\text{Eu}^{3+}$  phosphor for light-emitting diodes and field emission display. *J. Alloy. Compd.* **864**, 158840 (2021)
- Y.Q. Wang, Y.G. Wang, N. Chi, J.J. Yu, H.L. Shang, Demonstration of 575-Mb/s downlink and 225-Mb/s uplink bi-directional SCM-WDM visible light communication using RGB LED and phosphor-based LED. *Opt. Express* **21**, 1203–1208 (2013)
- F.B. Xiong, F.X. Xu, X.G. Meng, W.Z. Zhu,  $\text{Eu}^{3+}$ -activated  $\text{Ln}_2\text{TeO}_6$  ( $\text{Ln}=\text{La}, \text{Y}$ ) as a novel red emitting phosphor for warm white LEDs. *J. Mater. Sci: Mater. Electron.* **31**, 22945–22956 (2020)
- Z. Li, Q.L. Pian, L. Li, Y. Sun, S.S. Zheng, Luminescence properties of  $\text{SrBi}_2\text{B}_2\text{O}_7:\text{Eu}^{3+}$  orange-red phosphor. *Optik* **161**, 38–43 (2018)
- P. Du, X.Y. Huang, J.S. Yu, Facile synthesis of bifunctional  $\text{Eu}^{3+}$ -activated  $\text{NaBiF}_4$  red-emitting nanoparticles for simultaneous white light-emitting diodes and field emission displays. *Chem. Eng. J.* **337**, 91–100 (2018)
- W. Shi, A. Feng, H.B. Tang, Z.L. Ding, Y.Q. Ma, M.Z. Wu, G. Li, Preparation, characterization, and luminescence of  $\text{Eu}^{3+}$ -doped gadolinium tungstate,  $\text{Y}_3\text{Al}_5\text{O}_{12}:\text{Ce}$  phosphor, and their mixtures. *Opt. Mater.* **35**, 609–616 (2013)
- J.G. Li, H.F. Yan, F.M. Yan, Luminescence properties of a novel orange-red  $\text{CaBi}_2\text{B}_2\text{O}_7:\text{Eu}^{3+}$  phosphors for the near-UV pumped W-LEDs. *Optik* **21**, 10818–10822 (2011)
- R. Wang, J. Xu, C. Chen, Luminescent characteristics of  $\text{Sr}_2\text{B}_2\text{O}_5:\text{Tb}^{3+}, \text{Li}^+$  green phosphor. *Mater. Lett.* **68**, 307–309 (2012)
- W.X. You, Z.L. Xiao, F.Q. Lai, X.Y. Ye, Q. Zhang, H.H. Jiang, C.X. Wang, J.S. Liao, X.L. Liu, S.W. Zhong, Synthesis and photoluminescence properties of  $\text{Ba}_3\text{Al}_2\text{O}_6:\text{Eu}^{3+}$  red phosphor. *J. Mater. Sci.* **51**, 5403–5411 (2016)
- W. Fan, Y. He, L. Long, Y. Gao, F. Liu, J. Liu, Multiplexed excitations  $\text{KGd}_{1-x}\text{Eu}_x(\text{MoO}_4)_2$  red-emitting phosphors with highly  $\text{Eu}^{3+}$  doping for white LED application. *J. Mater. Sci: Mater. Electron.* **32**, 6239–6248 (2021)
- W.R. Liu, C.H. Huang, C.P. Wu, Y.C. Chiu, Y.T. Yeh, T.M. Chen, High efficiency and high color purity blue-emitting  $\text{NaSrBO}_3:\text{Ce}^{3+}$  phosphor for near-UV light-emitting diodes. *J. Mater. Chem.* **21**, 6869–6874 (2011)
- Z. Li, S.S. Zheng, X. Yang, B. Luo, S. Li, Y. Sun, Q.J. Cheng, Luminescence properties of  $\text{Sr}_2\text{MgB}_2\text{O}_6:\text{Tb}^{3+}, \text{Li}^+$  green-emitting phosphor. *J. Rare Earth.* **35**, 211–216 (2017)
- L.H. Tian, B.Y. Yu, C.H. Pyun, H.L. Park, S.I. Mho, New red phosphors  $\text{BaZr}(\text{BO}_3)_2$  and  $\text{SrAl}_2\text{B}_2\text{O}_7$  doped with  $\text{Eu}^{3+}$  for PDP applications. *Solid State Commun.* **129**, 43–46 (2004)
- Z. Zhang, W.J. Tang, Tunable luminescence and energy transfer of  $\text{Ce}^{3+}/\text{Eu}^{2+}/\text{Mn}^{2+}$ -tridoped  $\text{Sr}_8\text{MgLa}(\text{PO}_4)_7$  phosphor for white light LEDs. *J. Alloy. Compd.* **663**, 731–737 (2016)
- S.R. Anishia, M.T. Jose, O. Annalakshmi, V. Ramasamy, Thermoluminescence properties of rare earth doped lithium magnesium borate phosphors. *J. Lumin.* **131**, 2492–2498 (2011)
- K. Lemański, M. Stefański, D. Stefańska, P.J. Dereń, Luminescent properties of  $\text{Eu}^{3+}$  ions in  $\text{CaB}_6\text{O}_{10}$  polycrystals. *J. Lumin.* **159**, 219–222 (2015)
- I.E. Kolesnikov, R.S. Bubnova, A.V. Povolotskiy, Y.P. Biryukov, A.V. Povolotckaia, O. YuShorets, S.K. Filatov, Europium-activated phosphor  $\text{Ba}_3\text{Lu}_2\text{B}_6\text{O}_{15}$ : Influence of isomorphic substitution on photoluminescence properties. *Ceram. Int.* **47**, 8030–8034 (2021)
- B.R. Judd, Optical absorption intensities of rare-earth ions. *Phys. Rev.* **127**, 750 (1962)
- G.S. Ofelt, Intensities of crystal spectra of rare-earth ions. *J. Chem. Phys.* **37**, 511–520 (1962)
- T. Nagai, M. Ihara, Crystal structure of di-strontium borocaluminate,  $(\text{SrO})_2\text{-Al}_2\text{O}_3\text{-B}_2\text{O}_3$ . *J. Ceram. Soc. Jpn.* **80**, 432–437 (1972)
- G. Blasse, Energy transfer in oxidic phosphors. *Phys. Lett. A* **28**, 444–445 (1968)
- J.H. Zheng, Q.J. Cheng, S.Q. Wu, Z.Q. Guo, Y.X. Zhuang, Y.J. Lu, Y. Li, C. Chen, An efficient blue-emitting  $\text{Sr}_5(\text{PO}_4)_3\text{Cl}:\text{Eu}^{2+}$  phosphor for application in near-UV white light-emitting diodes. *J. Mater. Chem. C* **3**, 11219–11227 (2015)
- M.Y. Qu, X.Y. Zhang, X.Y. Mi, H.Y. Sun, Q.S. Liu, Z.H. Bai, Novel and wide-ranging color tuning photoluminescence properties of  $\text{Tb}^{3+}/\text{Eu}^{3+}$  doped garnet-type  $\text{Li}_3\text{Lu}_3\text{Te}_2\text{O}_{12}$  phosphor: energy transfer and enhanced thermal stability. *J. Alloy. Compd.* **872**, 159506 (2021)
- D.L. Dexter, J.H. Schulman, Theory of concentration quenching in inorganic phosphors. *J. Chem. Phys.* **22**, 1063–1070 (1954)
- V. Paterlini, F. Piccinelli, M. Bettinelli,  $\text{Tb}^{3+} \rightarrow \text{Eu}^{3+}$  energy transfer processes in eulytite  $\text{A}_3\text{Tb}(\text{PO}_4)_3$  ( $\text{A}=\text{Sr}, \text{Ba}$ ) and silico-carnotite  $\text{Ca}_3\text{Tb}_2\text{Z}_3\text{O}_{12}$  ( $\text{Z}=\text{Si}, \text{Ge}$ ) materials doped with  $\text{Eu}^{3+}$ . *Physica B* **575**, 411685 (2019)
- J.H. Zheng, Q.J. Cheng, S.Q. Wu, R. Chen, L.H. Cai, C. Chen, Electronic structure and luminescence properties of

- Tb<sup>3+</sup>-activated NaBaBO<sub>3</sub> green-emitting phosphor. *J. Rare Earth*. **33**, 933–938 (2015)
28. S.P. Lee, T.S. Chan, T.M. Chen, Novel reddish-orange-emitting BaLa<sub>2</sub>Si<sub>2</sub>S<sub>8</sub>: Eu<sup>2+</sup> thiosilicate phosphor for LED lighting. *ACS Appl. Mater. Inter.* **7**, 40–44 (2015)
29. M. Schwaab, J.C. Pinto, Optimum reference temperature for reparameterization of the Arrhenius equation. Part I: problems involving one kinetic constant. *Chem. Eng. Sci.* **62**, 2750–2764 (2007)
30. J.H. Li, Q.Y. Liang, Y.F. Cao, J. Yan, J.B. Zhou, Y.Q. Xu, L. Dolgov, Y.Y. Meng, J.X. Shi, M.M. Wu, Layered structure produced nonconcentration quenching in a novel Eu<sup>3+</sup>-doped phosphor. *ACS Appl. Mater. Inter.* **10**, 41479–41486 (2018)
31. B. Fan, W.X. Zhou, S.M. Qi, W.Y. Zhao, Eu<sup>3+</sup>-doped NaYGeO<sub>4</sub>: a novel red-emitting phosphors for ultraviolet or blue chips excited white LEDs. *J. Solid State Chem.* **283**, 121158 (2020)
32. H. Gao, J.F. Zhao, Y. Zhang, X.W. Zhang, H.X. Bu, Z.W. Zhao, X.Y. Song, X.Z.F. Yang, J.Y. Sun, Synthesis and photoluminescence of high color purity red-emitting BaLaLiTeO<sub>6</sub>: Eu<sup>3+</sup> phosphors. *J. Appl. Phys.* **129**, 143102 (2021)
33. A.P. Shablinskii, I.E. Kolesnikov, R.S. Bubnova, A.V. Povolotskiy, E. Lahderanta, S.K. Filatov, A novel thermally stable Ba<sub>3</sub>Bi<sub>2</sub>(BO<sub>3</sub>)<sub>4</sub>: Eu<sup>3+</sup> red phosphor for solid state lighting application. *J. Lumin.* **216**, 116714 (2019)
34. H. Tang, Y. Li, R. Yang, W. Gao, Phase formations and red-luminescence enhancement of Eu<sup>3+</sup>-activated NaBaY(BO<sub>3</sub>)<sub>2</sub> phosphors. *J. Lumin.* **208**, 253–258 (2019)
35. S. Long, J. Hou, G. Zhang, F. Huang, Y. Zeng, High quantum efficiency red-emission tungstate based phosphor Sr(La<sub>1-x</sub>Eu<sub>x</sub>)<sub>2</sub>Mg<sub>2</sub>W<sub>2</sub>O<sub>12</sub> for WLEDs application. *Ceram. Int.* **39**, 6013–6017 (2013)
36. B. Liu, X. Xiao, J. Yu, D. Mao, G. Lu, Influence of synthesis conditions on the morphologies of ReBO<sub>3</sub> microstructures and white light emission of YBO<sub>3</sub>:Eu<sup>3+</sup> phosphors prepared by an oleic acid-assisted hydrothermal method. *RSC Adv.* **6**, 69442–69453 (2016)
37. D.H. Sliney, Radiometric quantities and units used in photobiology and photochemistry: recommendations of the Commission Internationale de l'Eclairage (International Commission on Illumination). *Photochem. Photobiol.* **83**, 425–432 (2007)
38. S.D. Lei, B.J. Liu, Y. Gao, X.Y. Dong, Y.J. Gong, J. Xu, Y.X. Xu, D. Wang, Z.Q. Guo, T.Z. Wu, C.L. Zhou, Z.J. Cai, Y.J. Lu, Z. Chen, Investigation on circadian action and color quality in laser-based illuminant for general lighting and display. *IEEE Photonics J.* **12**, 8200509 (2020)
39. W. Davis, Y. Ohno, Color quality scale. *Opt. Eng.* **49**, 033602 (2010)

**Publisher's Note** Springer Nature remains neutral with regard to jurisdictional claims in published maps and institutional affiliations.

Springer Nature or its licensor (e.g. a society or other partner) holds exclusive rights to this article under a publishing agreement with the author(s) or other rightsholder(s); author self-archiving of the accepted manuscript version of this article is solely governed by the terms of such publishing agreement and applicable law.